ISSN 0965-545X, Polymer Science, Series A, 2020, Vol. 62, No. 6, pp. 670–679. © Pleiades Publishing, Ltd., 2020.

POLYMER BLENDS

Mullins Effect and Its Reversibility for Thermoplastic Vulcanizates Based on Ethylene–Acrylic Acid Copolymer/Nitrile–Butadiene Rubber Blends

Yingtao Sun[a], Linji Yang[a], Feifei Liu[a], and Zhaobo Wang[a,*]

[a]*College of Materials Science and Engineering, Qingdao University of Science and Technology, Qingdao, 266042 China*

**e-mail: wangzhb.cn@gmail.com*

Received March 30, 2020; revised May 5, 2020; accepted July 3, 2020

Abstract—Mullins effect during uniaxial cyclic compression tests, together with its reversibility, of ethylene–acrylic acid copolymer (EAA)/nitrile–butadiene rubber (NBR) thermoplastic vulcanizates (TPVs) were investigated systematically. The results showed that EAA/NBR TPVs had excellent mechanical properties when the weight ratio was 40/60. Morphology studies showed that sphere-like NBR particles were dispersed evenly in the etched TPVs surface with diameters of 5–8 μm. The experimental results of Mullins effect indicated that a stress softening phenomenon in the stress–strain curves of EAA/NBR TPVs during the uniaxial loading–unloading cycles could be observed obviously; moreover, the reversibility of Mullins effect could be significantly enhanced by increasing heat treatment temperature.

DOI: 10.1134/S0965545X20060103

INTRODUCTION

Thermoplastic vulcanizates (TPVs), a thermoplastic/rubber blend in which rubber components are cross-linked, is produced via dynamic vulcanization [1]. As a typical of elastomer, TPVs have been receiving growing focuses on industrial practicability due to the combination of the recyclability of thermoplastics and the excellent elastic restoring force of conventional rubbers [2, 3]. In addition, dynamic vulcanization is a more direct method to prepare a polymer material with convenience, efficiency and good mechanical properties compared with complicated chemical synthesis [4]. In situ reaction between the thermoplastic and rubber during dynamic vulcanization to form copolymers at the interface can effectively improve the compatibility and interfacial adhesion of the TPVs [5].

In general, TPVs can offer a substantial economic advantage with respect to the fabrication of products due to its unique characteristics. Over the past three decades, TPVs played an important role in the applications of automotive, buildings and constructions, wires and cables, etc [6, 7]. However, despite the reformatory progress dynamic vulcanization has made in the recent years, it still remains of great importance for the research on Mullins effect of TPVs in providing a good mechanical model for the complex behavior of industrial rubber. In order to control the properties of TPVs effectively, the study related to this unique behavior is an issue of major importance.

An important and intriguing characteristic of the mechanical properties of vulcanized rubber composites is that the required stress under the same certain strain is significantly decreased during the cyclic deformations, which is commonly known as the stress softening phenomenon or Mullins effect [8]. To provide a good mechanical model for the complex behavior of industrial rubber-like materials, phenomenological and macromolecular models have been proposed including bond rupture [9], molecules slipping [10], filler rupture [11], disentanglement [12], and double-layer model [13]. But until now, even though the Mullins effect has been studied for more than seventy years, it is still considered as a major challenge to provide good mechanical modeling of the complex behavior of industrial rubber-like materials [14]. Mullins effect could not only be observed in uniaxial tension, but also in uniaxial compression [15], hydrostatic tension [16], simple shear [17], and equi-biaxial tension [18, 19] etc. The subject of the cyclic uniaxial tensile behavior attracts most of those researchers, while the cyclic uniaxial compression behavior and the strengthening effect of stress-softening phenomenon is only attended by few researchers, as the research our group work, the behavior of HIPS/SBR, EVA/NBR, and HDPE/EPDM under the cyclic uniaxial compression was investigated systematically [20].

Ethylene–acrylic acid copolymer (EAA) is a thermoplastic resin with the merits of excellent adhesion and easy processing, which is widely used in packaging, adhesives, sealing and other industries; moreover,

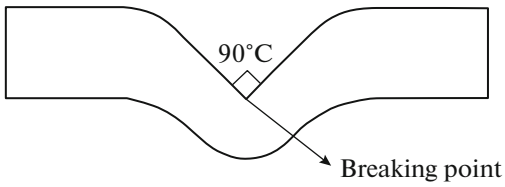

Scheme 1.

EAA is a polar polymer [21, 22] which consists of polar acrylic acid and non-polar ethylene. Nitrile–butadiene rubber (NBR) is a kind of polar unsaturated rubber composed of butadiene and acrylonitrile, which has the excellent properties of oil resistance, heat resistance and adhesion [23], and has been widely used in automotive, aerospace, petroleum, photocopying and other industries. To our best knowledge, there is no report on the preparation and application of EAA/NBR TPVs so far.

In this paper, we reported the preparation of EAA/NBR TPVs via dynamic vulcanization, where the mechanical properties, morphological properties, Mullins effect and its reversibility under heat treatment were investigated systematically.

EXPERIMENTAL

Materials

The ethylene–acrylic acid copolymer (EAA), grade 300 (acrylic acid content: 9.7 wt %), was commercially obtained from Dow Chemical Co. Ltd., US, with a melt index (MFI) of 8.5 g 10 min^{-1} (190°C, 2.16 kg^{-1}). The nitrile–butadiene rubber (NBR), grade 3305 (acrylonitrile content: 35 wt %), was commercially manufactured by Lanzhou Petrochemical Co. Ltd., China, with the Mooney viscosity (ML_{1+4} (100°C)) of 45. Dicumyl peroxide (DCP), used as a vulcanizing agent, was obtained from Gaoqiao Petrochemical Co., Ltd., China. Triallyl isocyanurate (TAIC) was used as a crosslinking agent and obtained from Rhein Chemie Co. Ltd., China. Antioxidant D was used as an antioxidant and obtained from Shengao Chemical Co., Ltd., Caoxian, China.

Preparation of Dynamically Vulcanized EAA/NBR Blends

Commercially available EAA, NBR and the industry raw materials, as above, were used for the TPVs. The concentration for cross-linking the NBR system was expressed in parts per hundred NBR rubbers by weight (phr). The formula of NBR rubber system using DCP as cross-linking agent was shown by weight (phr) as below: 100 phr NBR, 2 phr DCP, 3 phr TAIC, 1 phr Antioxidant D.

The dynamically vulcanized EAA/NBR blends were mainly prepared via the following two-step mixing process. In the first step, the preblend containing NBR and the cross-linking ingredients was compounded in a two-roll mill (SY-6215, Shiyan Precision Instrument Co. Ltd., China) at room temperature, and the preblend was removed from the mixer after 3 min of mixing. In the second step, the TPVs compounds were prepared by melt-mixing the NBR preblend with EAA resins and the EAA/NBR blending ratio was controlled in the range of 20/80 to 60/40. The mixer temperature was maintained at 165°C with a constant rotor (cam type) speed of 43 rpm. The requisite quantity of EAA resin was charged into the mixer and allowed to fully melt, and the NBR based preblend was added after 3 min. The mixing was continued for another 8 min to allow the dynamic vulcanization and finally the compound was removed from the mixer. The compound was compression molded in a plate vulcanizing machine (50 T, Shanghai Qun Yi Rubber Machinery Co. Ltd., China) under a pressure of 15 MPa at 170°C for 6 min, followed by cold compression in another machine (SK2401, Kai Yuan Machinery Co. Ltd., China) under a pressure of 15 MPa for 8 min at room temperature. The test specimens were die-cut from the compression-molded sheet and all specimens were used for testing after 24 h.

Mechanical Properties

According to ASTM D412, the dumbbell-shaped specimens for the measurement of tensile properties were prepared. The tearing strength was tested according to ASTM D624 using unnotched right angle test pieces. Both tensile and tearing tests were stretched on a universal testing machine (TCS-2000, GoTech Testing Machines Inc., China) at a crosshead speed of 500 mm/min until the specimens ruptured. The Shore A hardness was determined using a hand-held Shore A Durometer (LX-A, Shanghai Liu Ling Instrument Factory, China) according to ASTM D2240. Both the tearing strength and Shore A hardness were tested using unnotched right angle test pieces. The schematic diagram of unnotched right angle test pieces was shown in Scheme 1. Tensile set at break was tested according to ASTM D412 and Tensile set (100% elongation) was tested according to ASTM D1566. The average value of tensile strength was calculated for 5 test specimens and that of tearing strength, Shore A hardness and Tensile set (100% elongation) were calculated for 3 test specimens at room temperature.

Microscopy Analysis

Morphological study was carried out using field-emission scanning electron microscopy (FE-SEM, JEOL-6700F, Japan Electron Co. Ltd., Japan). For the etched surface of TPV samples, the EAA resin was extracted by immersing the blends into boiling xylene at 130°C for 3 h, and then the etched samples were ultrasounded for 5 min and dried in vacuum oven at

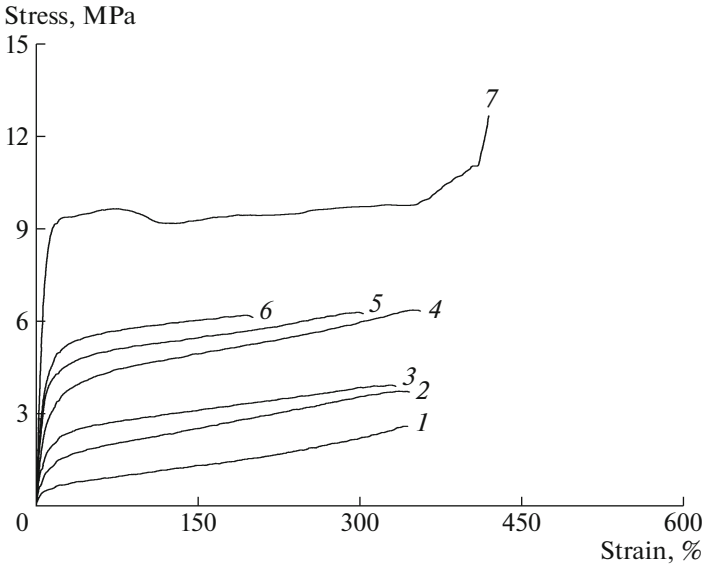

Fig. 1. Stress-strain curves of (*1*) NBR vulcanizate and dynamically vulcanized EAA/NBR blends: (*2*) 20/80, (*3*) 30/70, (*4*) 40/60, (*5*) 50/50, (*6*) 60/40, and (*7*) pure EAA.

40°C for 12 h. Finally, the samples were sputtered with thin layers of platinum and imaged using the FE-SEM.

Mullins Effect

In order to illustrate the material softening resulting from the Mullins effect, cyclic uniaxial compressive tests were performed on EAA/NBR TPVs (20/80 to 60/40 weight ratio) with a TCS-2000 universal tensile machine (GoTech Testing Machines Inc., China) operated in a local strain control mode. For a given cylindrical specimen, a cyclic uniaxial compression test was performed with a maximum strain increasing from 10 to 50% every 5 cycles and run at a low constant strain rate of 0.0083 s^{-1}. The compressive stress-strain curves during the loading and unloading period were measured.

Reversibility Behavior of the Mullins Effect

The reversibility behavior of Mullins effect of EAA/NBR TPVs was also investigated. In the first step, the sample was submitted to a cyclic uniaxial compression with given strain on the universal tensile machine. The strain was sequentially increased from 10 to 50% after each uniaxial compression cycle. The second step was to heat-treat the sample under different temperatures for 30 min in a vacuum oven after the cyclic uniaxial test, and then the sample was removed from the vacuum oven and cooled to room temperature. In the last step, the sample was submitted to a cyclic uniaxial compression with the same given strain again. The compressive stress-strain curves during the loading and unloading period were measured.

RESULTS AND DISCUSSION

Mechanical Properties of the Dynamically Vulcanized EAA/NBR Blends

The stress-strain curves of pure EAA, NBR vulcanizate, and dynamically vulcanized EAA/NBR blends at different weight ratios are shown in Fig. 1. The stress-strain curve of pure EAA in Fig. 1 shows that a typical deformation processes of tough plastic during the uniaxial tension could be found which included the elastic deformation, yield point, strain softening, and large deformation behavior obviously, indicating the hard and tough characters of EAA resin; while the stress-strain curve of NBR vulcanizate showed the elastomeric character of being soft and tough. The stress-strain curves of dynamically vulcanized EAA/NBR blends were similar in the shape of their curves and exhibited the representative elastomer with soft and tough character.

Table 1 shows the mechanical properties of pure EAA, NBR vulcanizate and the dynamically vulcanized EAA/NBR blends at series weight ratios. As can be seen in Table 1, the tensile strength and elongation at break of the dynamically vulcanized EAA/NBR blends reached a maximum value at 40 phr EAA incorporation. The EAA content had a significant effect on the tearing strength and shore A hardness, both of which increased linearly with the increasing of EAA content, indicating that the content of EAA was a major factor determining the mechanical properties of the blends.

The tensile set at break increased significantly with increasing EAA loading when the EAA content was below 50 phr; however, all the tensile set (100% elongation) values were less than 50%; the dynamically

Table 1. Mechanical properties of pure EAA, NBR vulcanizate, dynamically vulcanized EAA/NBR blends

EAA/NBR, weight ratio	Tensile strength, MPa	Elongation at break, %	Tensile set at break, %	Tearing strength, kN/m	Shore A hardness	Tensile set (100% elongation), %
0/100	2.6	342	2.5	9.1	44	/
20/80	3.7	346	55.0	25.0	56	20
30/70	4.0	332	115.0	35.1	71	30
40/60	6.4	357	170.0	49.4	82	45
50/50	6.3	302	160.0	53.0	86	45
60/40	6.2	199	80.0	57.4	89	35
100/0	12.6	421	385.0	100.1	90	/

vulcanized EAA/NBR blends could be described as elastomers according to the standard of ASTM D1566 standard.

As we know, the main structural units of EAA and NBR molecules are acrylic acid and acrylonitrile, all of which have strong polarity, resulting in the well compatibility and the strong interface interaction in the EAA/NBR blends, which is contributed to the high mechanical properties of the EAA/NBR blends.

Morphology and Microstructure of EAA/NBR TPVs

The FE-SEM image of the tensile fracture surfaces of EAA/NBR TPVs with 40/60 weight ratio prepared by dynamic vulcanization are shown in Fig. 2. The rough structure indicated that the tensile fractured surfaces of EAA/NBR TPVs consisted of numerous strip-like fibers, the tearing strips will generate and result in the large energy consumption; however, no rubber particles were observed on the fracture surface due to the firm adhesion and coverage of the EAA matrix. It could also be seen in Fig. 2 that there was no obvious phase separation in the surface, indicating that EAA phase had good compatibility with NBR phase.

During the process of dynamic vulcanization, the viscosity of the NBR increased quickly due to the initiation of the cross-linking reaction and then the NBR phase was gradually broken down into dispersed particles under the shear force. In our experiment, the EAA matrix phase in the surface of EAA/NBR TPVs with 40/60 weight ratio was extracted by etching TPVs with xylene and the FE-SEM images of the etched surfaces are shown in Fig. 3. As can be seen from Fig. 3, the vulcanized rubber domains remained undissolved and adhered to the surface with the diameter of about 5 to 8 μm. It could also be found that the crosslinked NBR particles, with irregular morphologies, were dispersed evenly in the thermoplastic matrix.

Mullins Effect of EAA/NBR TPVs

Figure 4 shows the stress-strain curves of EAA/NBR TPVs submitted to five cycles uniaxial loading-unloading compression tests with the given stain which was 10, 20, 30, 40, 50%, respectively (five cycles of loading-unloading from zero stress up to the

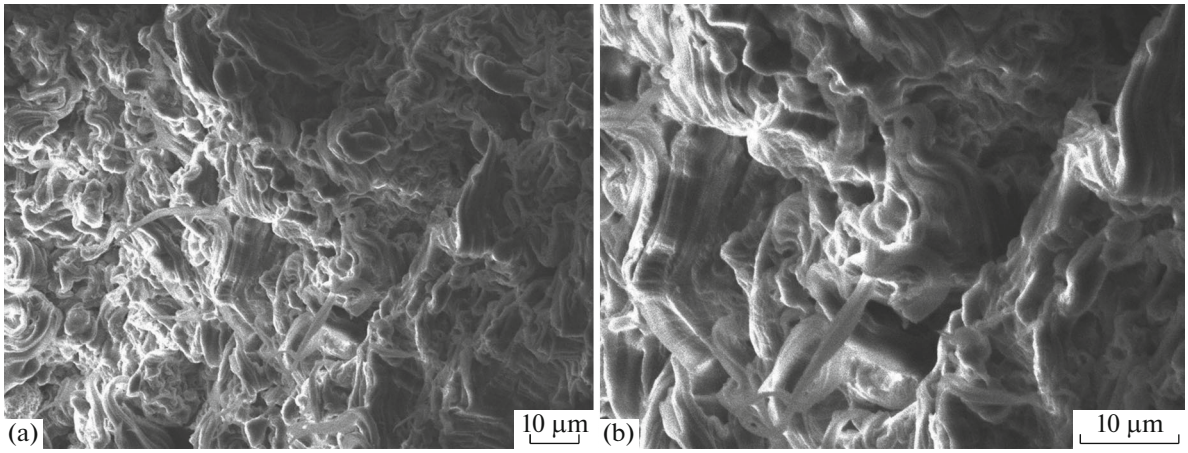

Fig. 2. FE-SEM of tensile fracture surfaces of EAA/NBR TPVs with 40/60 weight ratio: (a) ×1000, (b) ×2000.

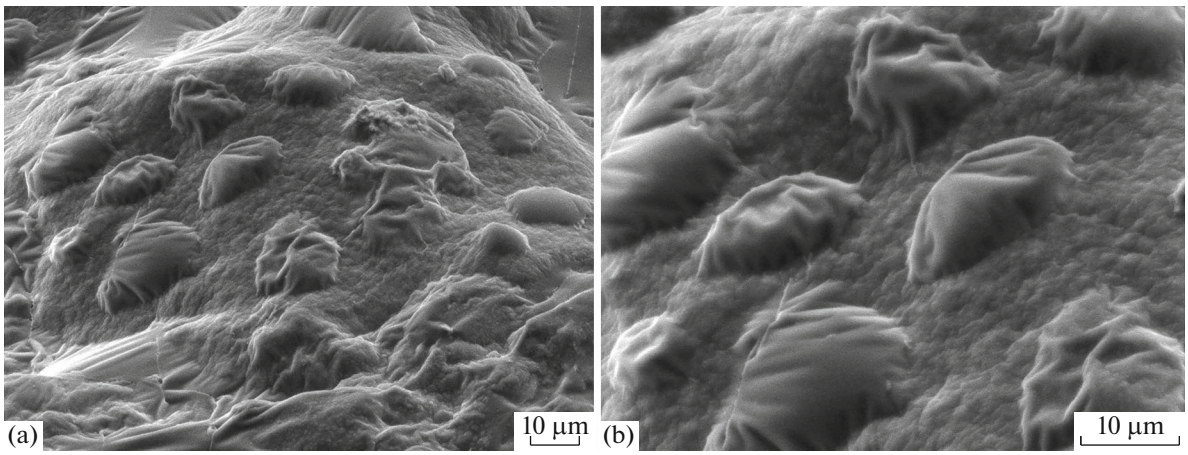

Fig. 3. FE-SEM of etched surfaces of EAA/NBR TPVs with 40/60 weight ratio: (a) ×1000, (b) ×2000.

maximum strain down to zero stress). From Fig. 4, a softening phenomenon could be observed that is specific to materials exhibiting the Mullins effect and the softening appeared obviously after the second loading-unloading cycle. It could also be seen that when the compression exceeded the maximum strain previously applied, the stress-strain response followed the same return path as that of the monotonous uniaxial tension test, indicating that previous strain had little influence on the stress-strain properties at greater strain. Moreover, the softening phenomenon was enhanced with increasing EAA content in TPVs, which could be clearly demonstrated from the increasing deviation degree between loading and unloading curves [24].

The maximum stress of EAA/NBR TPVs with 40/60 weight ratio as a function of the number of the loading-unloading cycles under different compression strain are shown as Fig. 5a. It could be seen in Fig. 5a that the stress-softening phenomenon under larger strain was more obvious than that under smaller strain; moreover, the maximum stress could be found under the first loading with given strain, and then it decreased slightly in subsequent cycles. To characterize the uniaxial tensile behavior, Mullins and Tobin [25] proposed a microstructural model, the stress-softening virgin material consisted of an amorphous mixture containing a hard phase and a soft phase microstructure, most of the deformation occurred in the soft phase and the extent of the damage depended on the maximum previous strain experienced by the materials. In our experiment, the EAA, as a hard phase, was the matrix of the blends; during the first loading, the plastic deformation and the tearing strips of EAA matrix would generate and result in the large energy consumption. During the subsequent loading-unloading cycles, most deformations took place in the soft regions of the NBR, and the hard regions of the EAA matrix made little contribution to the deformation, but they may be broken to form soft regions during first loading, after the previous cycle, the contribution of hard region in deformation was relatively small and the measured stress at a given strain was mainly exerted to the soft region; therefore, the maximum stress values decreased slightly at the later cycles after the second loading.

Figure 5b illustrated the residual deformation of EAA/NBR TPVs with 40/60 weight ratio in the uniaxial loading-unloading cycles. Generally, one of the important features in Mullins effect was the accumulation of residual deformation as the deformation could not recover completely. It could be observed in Fig. 6b that residual deformation was increased obviously with increasing compression strain and loading-unloading cycles. It was easy to understand that large deformation required a large amount of energy and would result in relatively high residual deformation due to the large plastic deformation of the EAA matrix.

In order to investigate the internal friction loss during the loading-unloading compression tests, the integral results of the hysteresis rings were calculated by Origin 8.0 software [26], and the results are shown in the Fig. 6. From Fig. 6, it could be found that the maximum internal friction loss was generated in the first loading-unloading cycle and the internal friction loss was increased with the increase of compression strain; moreover, it was decreased obviously during the second loading-unloading cycle while only decreased slightly during the later loading-unloading cycles at given strain. It should be pointed out that the variation of internal friction loss was consistent with the variation of residual deformation as described above. During the first loading-unloading cycle, the plastic deformation of EAA matrix results in the large energy consumption and residual deformation, resulting in the relatively large hysteresis ring and internal friction loss; however, in the subsequent loading-unloading cycles, the measured stress under the same strain was mainly exerted to the soft phase and the

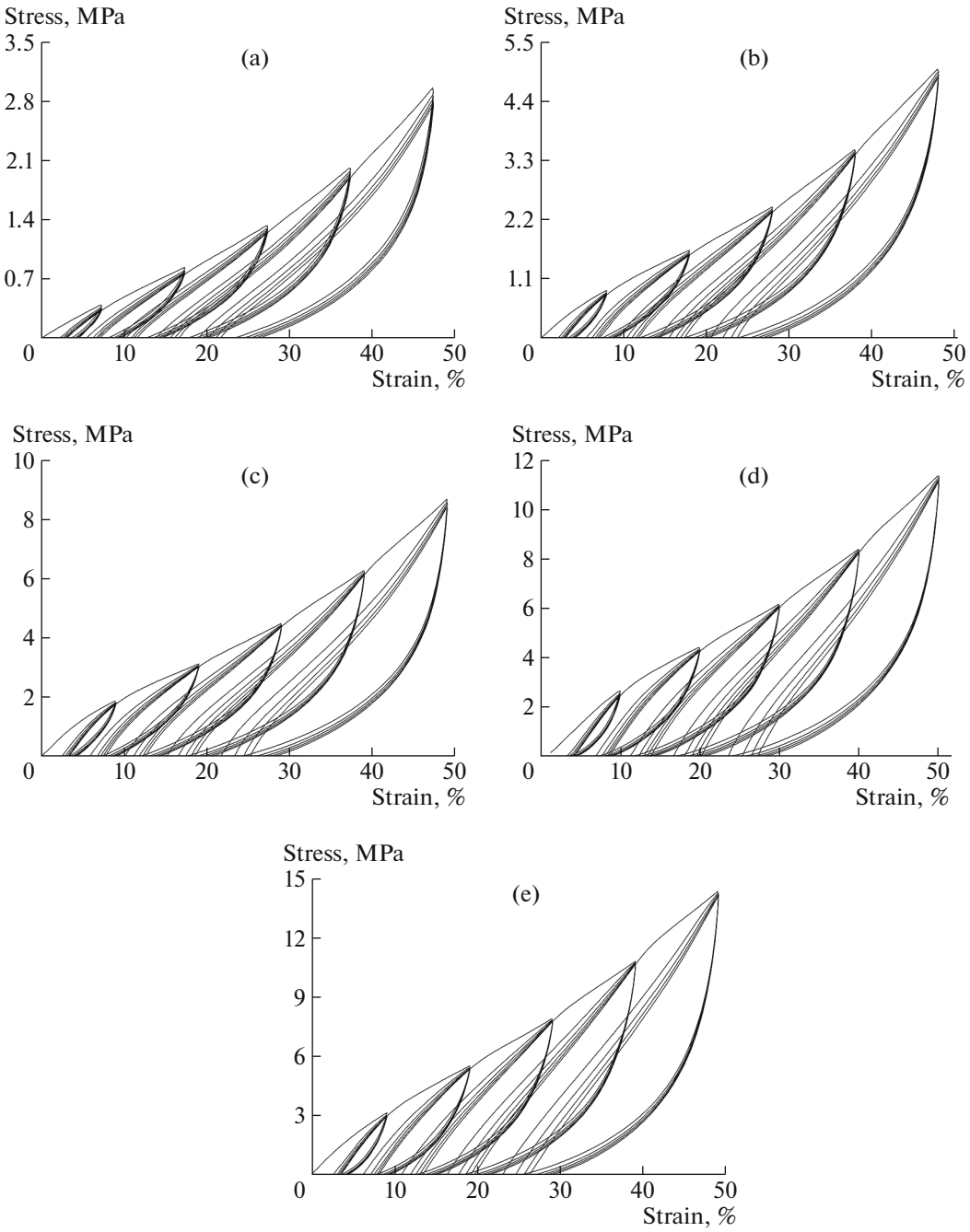

Fig. 4. Stress-strain curves of EAA/NBR TPVs submitted to 5 uniaxial loading-unloading cycles with given strain. EAA/NBR = (a) 20/80, (b) 30/70, (c) 40/60, (d) 50/50, (e) 60/40.

residual deformation only changed slightly, resulting in the lower internal friction loss.

In order to illustrate the stress softening phenomenon of EAA/NBR TPVs better, the integral results of the strain energy were calculated by Origin 8.0 software, and the degree of stress softening effect (D_S) can be calculated by following Eq. (1) [27]:

$$Ds(\%) = \frac{W_1(\varepsilon) - W_i(\varepsilon)}{W_1(\varepsilon)} \times 100\%, \quad (1)$$

where W_1 is the strain energy needed during the first loading at given strain and $W_i(\varepsilon)$ is the strain energy needed during *No.i* loading at given strain, and it is calculated by integrating the area surrounded by the horizontal axis and stress-strain curve during loading period. The results of D_s are shown in Fig. 7a, the more times the loading-unloading cycles at a given strain, the softer will be the TPVs, resulting in the significantly increasing of the D_s for a specific strain; moreover, the degree of stress softening effect was

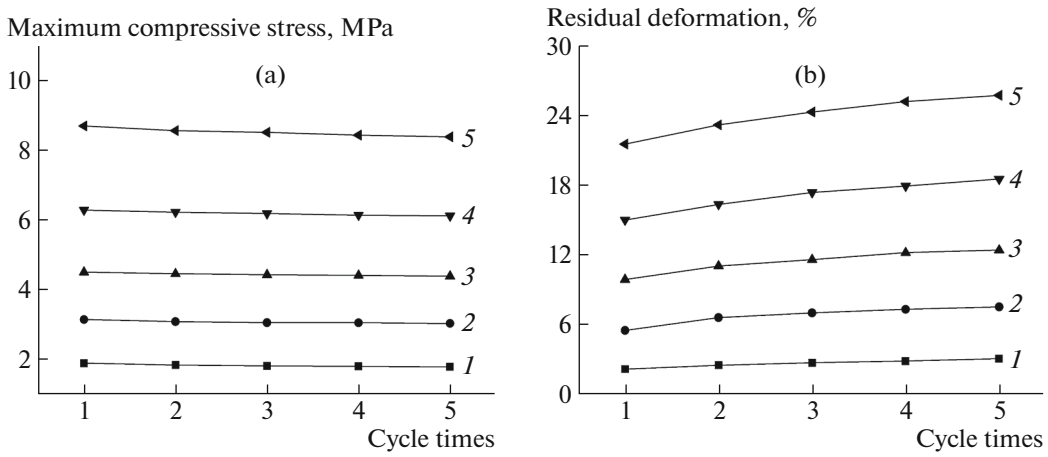

Fig. 5. Maximum compressive stress and residual deformation of EAA/NBR TPVs with 40/60 weight ratio as a function of the number of loading-unloading cycles. λ = (*1*) 10, (*2*) 20, (*3*) 30, (*4*) 40, (*5*) 50%.

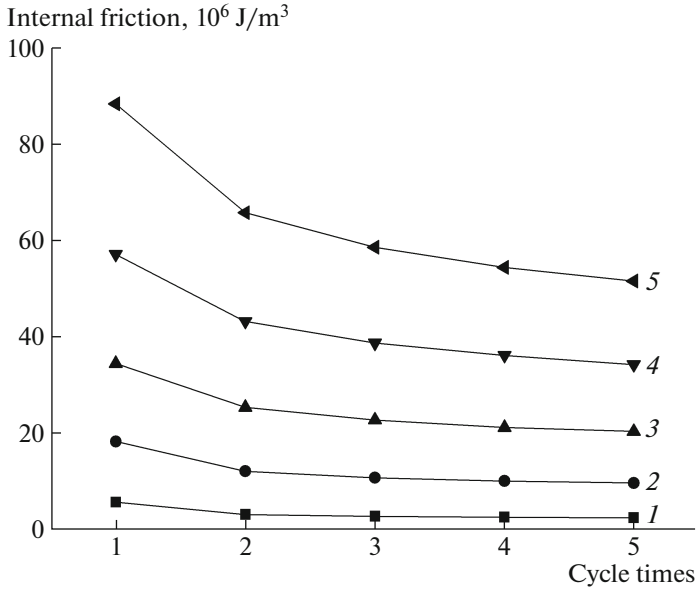

Fig. 6. Internal friction loss of EAA/NBR TPVs with 40/60 weight ratio as a function of the number of loading-unloading cycles. λ = (*1*) 10, (*2*) 20, (*3*) 30, (*4*) 40, (*5*) 50%.

decreased obviously with increasing compression strain.

To illustrate the Mullins effect more directly, the damping factor (tan δ) of the EAA/NBR TPVs can be expressed using following Eq. (2):

$$\tan\delta = \frac{E_i(\varepsilon)}{W_i(\varepsilon)}, \quad (2)$$

where $E_i(\varepsilon)$ represents the internal friction value of each cycle, namely the areas between loading-unloading cycle curves and *x*-axis in each cycle, while $W_i(\varepsilon)$ is the strain energy needed during the loading at given strain, which is calculated by integrating the area that surrounded by the horizontal axis and the stress-strain curve during loading period [28]. The degree of tanδ is shown in Fig. 7b. As can be seen in Fig. 7b the tanδ of EAA/NBR TPVs with 40/60 weight ratio were increased obviously with increasing compression strain, while they were constantly decreased with increasing loading-unloading cycles at given strain and changed slightly eventually.

Recovery Behavior of Mullins Effect of EAA/NBR TPVs

The recovery behavior of the Mullins effect has been observed through the reversibility of the permanent set or comparing the extent to which the two stress-strain curves are close to each other. Mullins studied the stress-recovery of filled NR which showed

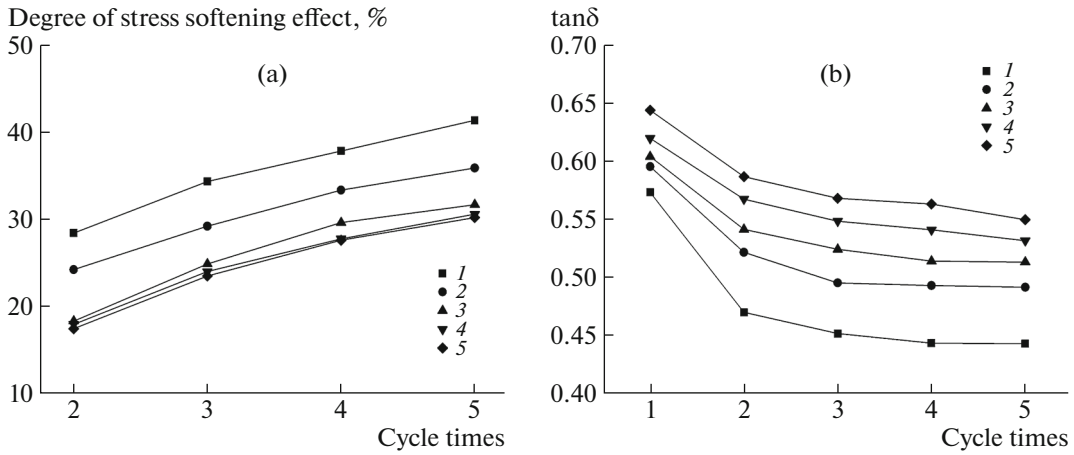

Fig. 7. (a) Degree of stress softening effect and (b) damping factor (tanδ) of EAA/NBR TPVs with 40/60 weight ratio as a function of the number of loading-unloading cycles. λ = (*1*) 10, (*2*) 20, (*3*) 30, (*4*) 40, (*5*) 50%.

a temperature-dependent feature of the reversibility. The influence of heat treatment on the recovery behavior of Mullins effect in cyclic compression test was researched, and the specimens were subjected to the heat treatment at different temperatures for 30 min after the first cyclic compression and then submitted to the second cyclic uniaxial compression, the stress-strain curves are shown in Fig. 8, the recovery behavior of Mullins effect can be observed by comparing the extent to which the two strain-stress curves are close to each other. It could be seen in Fig. 8 that the reversibility of Mullins effect showed a temperature-dependent feature and was enhanced with the increasing temperature. When the specimen was kept at room temperature after the first cyclic compression, the second cyclic compression curve showed a slight recovery behavior; however, the reversibility was enhanced remarkably when increasing the heat treatment temperature to 105°C, indicating the fine deformation reversibility of the EAA/NBR TPVs.

Table 2 shows the initial heights (h_0) and the heights (h) of specimens after heat treatment. Residual compression strain (K) can be calculated by following Eq. (3):

$$\mathrm{K}(\%) = \frac{h_0 - h}{h_0} \times 100\% \qquad (3)$$

It could be seen from Table 2 that the residual compression strain was 5.5% when the heat treatment temperature was 23°C; however, when the heat treatment temperature was raised to 105°C, it decreased to –0.6%, indicating that the deformation recovery ability of Mullins effect of TPV was improved obviously with increasing heat treatment temperature. Usually, Mullins effect is thought to be caused by Micro-damage accumulation [29], we could understand that the maximum stress at a specific strain could not achieve the value in the first loading-unloading cycle, indicating that the breaking of some weak molecular interactions and some chains; moreover, some micro-damage generated during the deformation became permanent and could not recover under our experimental conditions. However, under the heat treatment, the plastic deformation of thermoplastic resin could be recovered and the destroyed interface interaction in TPVs could also be recovered partially, leading to the partial healing of Mullins effect. When the specimens were subjected to the high temperature treatment after the first cyclic compression, the stress only could recover partially during the later cyclic uniaxial loading-unloading compression, indicating that even though rubber-plastic bonds were broken under large

Table 2. Residual compression strain of EAA/NBR TPVs under different heat treatment

Temperature, °C	Properties		
	initial height h_0, mm	height after heat treatment h, mm	residual compression strain, %
23	9.95	9.40	5.5
60	9.87	9.67	2.0
75	10.01	9.86	1.5
90	9.88	9.80	0.8
105	9.95	10.01	–0.6

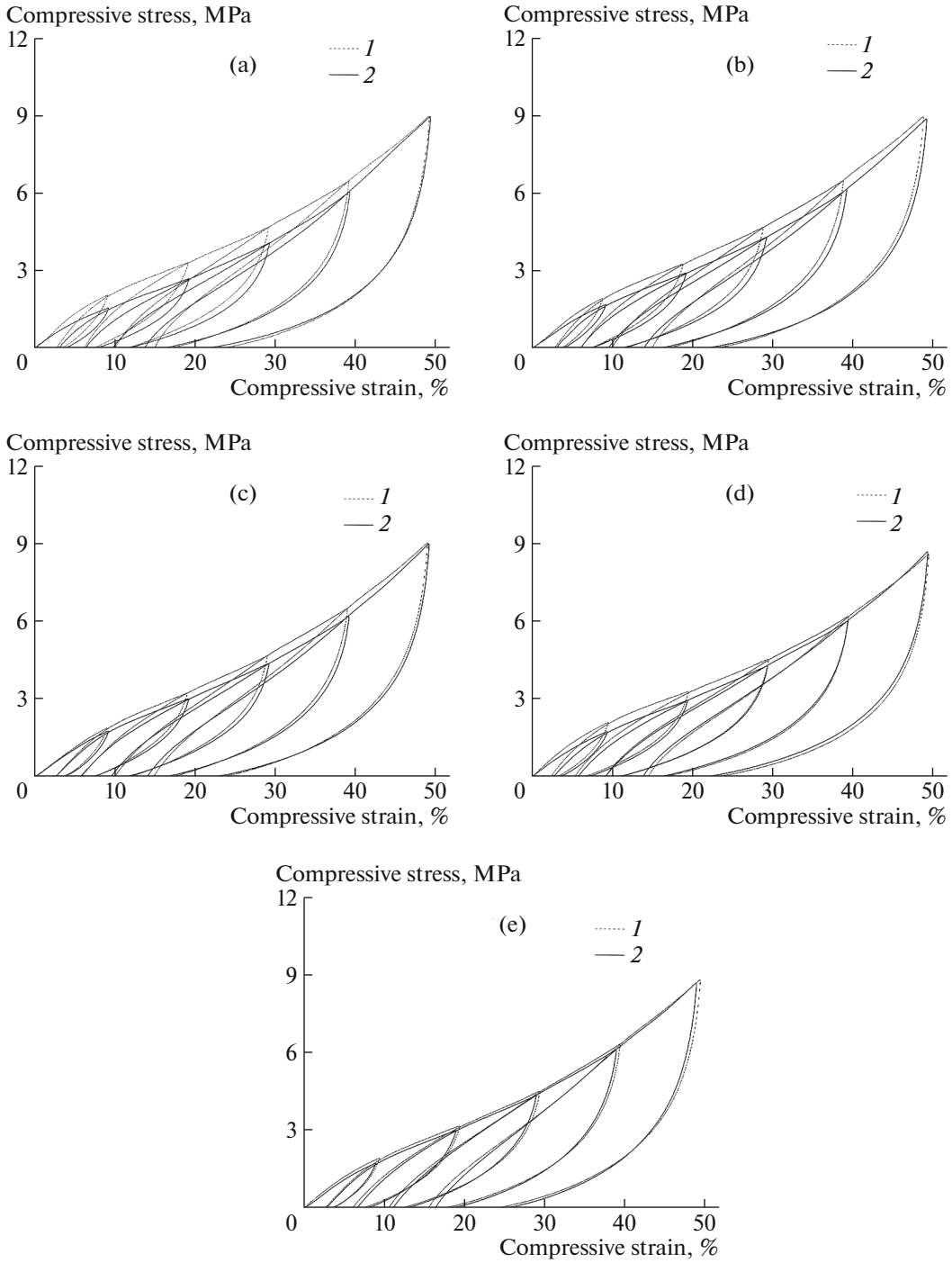

Fig. 8. Influence of heat treatment temperatures on the reversibility of Mullins effect of EAA/NBR TPVs with 40/60 weight ratio submitted to cyclic uniaxial compression under given strain. Heat treatment temperature: (a) 23, (b) 60, (c) 75, (d) 90, (e) 105°C. (*1*) First compress, (*2*) second compress.

deformation, the molecular interaction could also be regenerated under the high treatment temperature.

CONCLUSIONS

EAA/NBR TPVs with different weight ratios were prepared by dynamic vulcanization in the presence of the DCP and the mechanical properties and Mullins effect of the prepared blends were investigated systematically. The experimental results showed that increasing the content of EAA in the TPVs could contribute to the increase of tearing strength and hardness, while tensile strength and elongation at break both reached the maximum when the EAA content was 40 phr. FE-

SEM studies showed that the tensile fractured surface of EAA/NBR TPVs consisted of numerous tearing strips and there was no obvious phase separation on the fracture surfaces of the TPVs with 40/60 weight ratio, indicating the strong interface interaction between the EAA phase and the NBR phase. The NBR particles with average diameter of 5~8 μm were dispersed evenly in the etched surface of EAA/NBR TPVs. The Mullins effect was observed in our experiment, increasing compression strain and EAA content in TPVs could strengthen the Mullins effect. Moreover, the reversibility of Mullins effect showed a strong dependence on the heat treatment temperature, and increasing the heat treatment temperature could strengthen the reversibility of Mullins effect remarkably.

FUNDING

The work was supported by Shandong Provincial Natural Science Foundation, China (ZR2017MEM021) and Upgraded Project of Shandong Province for Guidance Ability of Graduate Tutors (SDYY17044).

CONFLCIT OF INTEREST

The authors declare that they have no conflict of interest.

REFERENCES

1. Y. K. Chen, D. S. Yuan, and C. H. Xu, ACS Appl. Mater. Interfaces **6**, 3811 (2014).
2. C. Xu, W. Wu, J. Nie, L. Fu, and B. Lin, Composites, Part A **117**, 116 (2019).
3. M. A. Roy, M. Duin, A. B. Spoelstra, and J. G. Goossens, Soft Matter **6**, 1758 (2010).
4. T. Zhao, W. Yuan, Y. Li, Y. Weng, and J. Zeng, Macromolecules **51**, 2027 (2018).
5. S. Datta, K. Naskar, J. Jelenic, and J. W. M. Noordermeer, J. Appl. Polym. Sci. **98**, 1393 (2005).
6. I. W. Small, P. Singhal, T. S. Wilson, and D. J. Maitland, J. Mater. Chem. **20**, 3356 (2010).
7. T. I. Medintseva, N. A. Erina, and E. V. Prut, Polym. Sci., Ser. A **50**, 647 (2008).
8. Z. H. Liu, F. J. Zeng, J. Du, X. Fan, Z. H. Zuo, and C. Y. Tao, J. Appl. Biomater. Funct. Mater. **44**, 2393 (2013).
9. A. F. Blanchard and D. Parkinson, Ind. Eng. Chem. **44**, 799 (1952).
10. R. Houwink, Rubber Chem. Technol. **29**, 888 (1956).
11. G. Kraus, C. W. Childers, and K. W. Rollmann, J. Appl. Polym. Sci. **10**, 229 (1996).
12. D. E. Hanson, M. Hawley, R. Houlton, K. Chitanvis, P. Rae, E. B. Orler, and D. A. Wrobleski, Polymer **46**, 10989 (2005).
13. Y. Fukahori, J. Appl. Polym. Sci. **95**, 60 (2005).
14. A. L. V. Svistkov and B. Lauke, Polym. Sci., Ser. A **50**, 591 (2008).
15. A. Amin, M. S. Alam, and Y. Okui, Mech. Mater. **34**, 75 (2002).
16. A. Dorfmann, Acta Mech. **165**, 117 (2003).
17. M. F. Beatty, Elasticity **59**, 369 (2000).
18. J. Li, D. Mayau, and V. Lagarrigue, J. Mech. Phys. Solids **56**, 953 (2008).
19. W. V. Mars, and A. Fatemi, J. Eng. Mater. Technol. **126**, 19 (2004).
20. Z. B. Wang, S. Li, D. Y. Wei, and J. Zhao, J. Thermoplast. Compos. **28**, 1154 (2015).
21. R. Scaffaro, F. P. La Mantia, and C. Castronovo, Macromol. Chem. Phys. **205**, 1402 (2004).
22. J. J. Liu, and Y. Zhang, Polym. Degrad. Stab. **96**, 2215 (2011).
23. M. M. Salehi, T. Khalkhali, and A. A. Davoodi, Polym. Sci., Ser. A **58**, 567 (2016).
24. C. C. Wang, Y. F. Zhang, and Z. B. Wang, J. Thermoplast. Compos. **30**, 827 (2017).
25. L. Mullins, and N. Tobin, Rubber Chem. Technol. **30**, 555 (1957).
26. L. Zhang, J. Hua, and Z. B. Wang, J. Polym. Res. **26**, 11 (2019).
27. L. Mullins, Rubber Chem. Technol. **42**, 339 (1969).
28. V. A. Kalinchev, Polym. Sci., Ser. C **49**, 115 (2007).
29. G. Marckmann, E. Verron, L. Gornet, G. Chagnon, P. Charrier, and P. Fort, J. Mech. Phys. Solids **50**, 2011 (2002).